Link Adaptation and Carriers Detection Errors in Multibeam Satellite Systems with Linear Precoding

Anxo Tato†, Stefano Andrenacci*, Symeon Chatzinotas*, Carlos Mosquera†
† atlanTTic Research Center, University of Vigo, Spain
{anxotato, mosquera}@gts.uvigo.es
* SnT - securityandtrust.lu, University of Luxembourg
{stefano.andrenacci, symeon.chatzinotas}@uni.lu

***Abstract*—The application of linear precoding at the gateway side enables broadband multibeam satellite systems to use more aggressive frequency reuse patterns increasing the overall capacity of future High Throughput Satellites (HTS). However, although some previous works about precoding consider imperfect CSIT (Chanel State Information at the Transmitter) adding some CSI estimation errors, that is not the main cause of CSI degradation. In practice, receivers can only detect and estimate a few coefficients of the CSI vector being the other nullified, replaced by zeros. This introduces errors in the SINR calculation by the gateway that lead to the assignment of Modulation and Coding Schemes (MCS) over the decoding possibilities of the users, increasing the rate of erroneous frames. In this work, the errors in the SINR calculation caused by the nullification of the CSI are analyzing statistically and geographically using a radiation diagram of 245 beams over Europe. Furthermore, a solution based on a link adaptation algorithm with a per user adaptive margin is proposed, helping to achieve the QEF (Quasi-error Free) target of DVB-S2X systems.**

I. Introduction

The use of more aggressive frequency reuse patterns, as full-frequency reuse, allows to increase the capacity of the forward link of multibeam satellite communications systems. This approach is proposed to increase the system capacity of High Throughput Satellites (HTS) operating at Ka-band. To mitigate the higher co-channel interference which arises in this scenario, linear precoding techniques reveal as a promising method to deal with it. Indeed, the new superframe format of DVB-S2X [1] enables the use of precoding in DVB broadband satellite systems.

Several works propose the application of linear precoding to the forward link of DVB-S2(X) based systems, as [2], [3], [4], [5] and [6]. Performance analysis and practical issues are addressed; among others, multiplexing of several users per frame, the importance of users scheduling in the final system capacity, the outdated CSIT (Channel State Information at the Transmitter), or CSI estimation errors.

However, there is an important problem related with imperfect CSI in precoding which previous works do not consider, the nullification effect. To the best of our knowledge this problem is only partially covered in [7], although not with as much detail as in this work. In precoded multibeam satellite systems the CSI of each user is not a scalar any more but a vector whose components are the channel estimates of the other interfering beams. It often happens that receivers are not able to estimate many of these channels since the interfering signals from other beams are received with a very low level. Therefore, the CSI available at the gateway is a sparse vector with many zero entries. This causes two problems. On the one hand, the calculated precoding matrix is not optimized for the actual channel but for the nullified version of the channel matrix, leading to some performance loss. And, more importantly, the Signal to Interference and Noise Ratio (SINR) calculated by the gateway for each user differs from the actual value. The error in the estimation of the users SINR by the gateway can be high enough to lead, in the case of overestimation, to increase the rate of erroneous frames over the QEF target of DVB-S2(X) systems, since the estimated SINR is used to perform Modulation and Coding Scheme (MCS or MODCOD) allocation.

This work tries precisely to fill the gap related to the nullification error problem found in the literature, explaining how nullification occurs, characterizing the statistical and geographical distribution of the SINR errors due to the nullification effect and proposing a method to overcome this problem. Since the nullification effect causes wrong MCS allocation due to the errors in the calculated SINR, a link adaptation algorithm is proposed as a countermeasure for frame errors that the nullification triggers. An Outer Loop Link Adaptation (OLLA) algorithm previously presented for single link mobile satellite systems [8] and dual polarization mobile satellite systems [9], is adapted here for reducing the side effects of the CSI nullification.

This paper is structured as follows. Section II presents the equations of the system model, describes the multibeam channel model and the computation of the precoding matrix and precoded SINRs. Then, Section III explains the different types of nullification and how they are modeled. Afterwards, the main results of the paper on the analysis of the SINR error due to nullification are collected in Section IV, which are obtained by means of simulations using data from a specific satellite beam pattern. Lastly, before the conclusions, Section V describes the link adaptation algorithm to overcome the problems caused by the nullification, and provides some simulation results showing how the proposed strategy solves the problem.

II. System model

We consider the forward link of a multibeam satellite communications system with full frequency reuse operating at Ka-band. Linear precoding is used to reduce the co-channel interference which arises in this configuration, significantly higher than that in four-color frequency/polarization configurations [4]. Let us assume that the satellite operates N beams with a single feed per beam (SFPB) payload. For the sake of simplicity, multicasting is not considered in this study, only N users are served at a time, one per beam. With all these considerations the general model for signals received at the User Terminals (UTs) at a given time instant in matrix notation is

$$\mathbf{y} = \mathbf{H}\mathbf{x} + \mathbf{n} = \mathbf{H}\mathbf{W}\mathbf{s} + \mathbf{n} \tag{1}$$

where the vector $\mathbf{y} \in \mathbb{C}^N$ collects the received signals by the set of all users, $\mathbf{s} \in \mathbb{C}^N$ are the information symbols for each user, which are normalized in terms of energy, $\mathbb{E}\{|s_k|^2\} = 1$, $\mathbf{x} \in \mathbb{C}^N$ are the precoded transmitted signals by each antenna, $\mathbf{W} \in \mathbb{C}^{N\times N}$ is the precoding matrix, $\mathbf{H} \in \mathbb{C}^{N\times N}$ is the channel matrix, and $\mathbf{n} \sim \mathcal{CN}(\mathbf{0}, N_0\mathbf{I}_N)$ is the noise term, complex zero mean Additive White Gaussian Noise (AWGN) measured at each UT receiving antenna.

A. Channel model

The general model [10] for the complex channel matrix is

$$\mathbf{H} = \mathbf{\Phi}_p\mathbf{B}\mathbf{\Phi}_{RF} \tag{2}$$

with $\mathbf{B}$ an $N \times N$ real matrix which models the link budget of each UT, and $\mathbf{\Phi}_p$ and $\mathbf{\Phi}_{RF}$ two diagonal complex $N \times N$ matrices which contain the phase terms arising in the signal propagation and the satellite RF chains, respectively. The real matrix $\mathbf{B}$ models each UT link budget and contains the satellite antenna radiation pattern, the path loss and the receive antenna gain. Its $i, j-$th entry is given by:

$$b_{ij} = \frac{\lambda}{4\pi d_k}\sqrt{G_R G_{ij}}, \tag{3}$$

with d_k the distance between the k-th UT and the satellite (slant range), λ the wavelength, G_R the receiver antenna gain and G_{ij} the multibeam antenna gain between the k-th single antenna UT located in the i-th beam and the j-th on board antenna feed.

The phase of the channel coefficients is divided in two terms. On the one hand, the diagonal matrix $\mathbf{\Phi}_p$ models the phase originated during the propagation. Here we assume that due to the big slant range the signals of all satellite antennas arrive at the UT with the same phase, this is the reason why this matrix multiplies $\mathbf{B}$ by the left. This phase is fixed for each user during all the simulations and it is uniformly distributed between all UTs. Their elements are $[\mathbf{\Phi}_p]_{nn} = e^{j\phi_n}$, where ϕ_n is an uniform random variable in $[0, 2\pi)$.

On the other hand, the diagonal matrix $\mathbf{\Phi}_{RF}$ models the random phase introduced by the local oscillators, which are independent for each payload chain, and therefore this matrix multiplies $\mathbf{B}$ by the right. The elements of this diagonal matrix are $[\mathbf{\Phi}_{RF}]_{nn} = e^{j\theta_n}$, with $\theta_n \sim \mathcal{N}(0, \sigma_\theta^2)$. A value of 20^o for the variance is used as suggested in [10]. Contrary to ϕ_n, which is fixed during all the simulations, θ_n change with each time realization (transmitted frame).

Lastly, the channel matrix $\mathbf{H}$ for a given time realization is built row by row with the channel vector of the scheduled users, $\mathbf{h}_k^\perp$, one per beam since only unicast is considered here. However, the gateway does not have access to the actual channel matrix $\mathbf{H}$ but to a matrix $\hat{\mathbf{H}}$ which includes the nullification effect as well as estimation errors. This will be explained in detail in the next section. A 245 beams multibeam channel, generated based on ESA's radiation pattern [5], is used in all the simulations. For each beam a grid with discrete positions is available, ranging the number of positions of the beams from 68 to 108.

B. Linear precoding

Let $\mathsf{snr} = P_n/N_0$ the per beam and per polarization transmit SNR, with P_n the average per beam and polarization transmit power and N_0 the noise power at each receiver. The MMSE (Minimum Mean Square Error) precoding matrix calculated by the gateway using the nullified imperfect CSIT $\hat{\mathbf{H}}$ is given by [11]

$$\mathbf{W}_{\text{mmse}} = \hat{\mathbf{H}}^H\left(\hat{\mathbf{H}}\hat{\mathbf{H}}^H + \frac{1}{\mathsf{snr}}\mathbf{I}_N\right)^{-1}. \tag{4}$$

In order to set the transmitted power, there are several options to normalize (4) like for example SPC (Sum Power Constraint), MPC (Maximum Power Constraint) or PLPC (Per Line Power Constraint). SPC, which is used in this paper, can be applied when the satellite payloads have Multiport Amplifiers (MPA) or Flexible TWTAs, that allow the total power (NP_n) to be shared among the different beams. In this case $\mathbf{W}_{\text{mmse}}$ is multiplied by a scaling factor

$$\eta = \sqrt{NP_n/\text{trace}\{\mathbf{W}_{\text{mmse}}\mathbf{W}_{\text{mmse}}^H\}} \tag{5}$$

becoming the final precoding matrix

$$\mathbf{W} = \eta\mathbf{W}_{\text{mmse}}. \tag{6}$$

C. Precoded SINRs

If we refer to the rows of $\mathbf{H}$ and $\hat{\mathbf{H}}$ as $\mathbf{h}_k^\perp$ and $\hat{\mathbf{h}}_k^\perp$, respectively, and to the columns of $\mathbf{W}$ as $\mathbf{w}_k$ (the precoding vectors), the precoded SINR for an UT at the k-th beam can be calculated as

$$\mathsf{sinr}_k = \frac{|\mathbf{h}_k^\perp\mathbf{w}_k|^2}{\sum_{j\neq k}|\mathbf{h}_k^\perp\mathbf{w}_j|^2 + N_0} \tag{7}$$

and the SINR which the gateway estimates for a user at the k-th beam using the Imperfect CSIT is

$$\hat{\mathsf{sinr}}_k = \frac{|\hat{\mathbf{h}}_k^\perp\mathbf{w}_k|^2}{\sum_{j\neq k}|\hat{\mathbf{h}}_k^\perp\mathbf{w}_j|^2 + N_0}. \tag{8}$$

We use the notation sinr_k and $\hat{\mathsf{sinr}}_k$ to refer to the real and estimated precoded linear SINRs and we reserve the capital letters for their counterpart in logarithmic scale:

$$\text{SINR}_k = 10\log_{10}\mathsf{sinr}_k \quad (dB) \tag{9}$$

$$\hat{\text{SINR}}_k = 10\log_{10}\hat{\mathsf{sinr}}_k \quad (dB). \tag{10}$$

As we are interested in the SINR errors caused by nullification and their impact on the MCS selection, in the following sections we will characterize the SINR absolute error, defined as

$$e_k = \hat{\text{SINR}}_k - \text{SINR}_k \ (dB). \tag{11}$$

This is the difference between the SINR estimated by the gateway for each UT (using $\mathbf{W}$ and $\hat{\mathbf{H}}$) and the real SINR that the UT undergoes (which depends on $\mathbf{W}$ and the actual channel $\mathbf{H}$). If e_k is positive it means that the gateway overestimates the SINR, so that if no appropriate margins are used in the MCS selection, transmission errors will take place as a result, even in the absence of other channel imperfections.

The selected metric to evaluate the nullification problem is the SINR in dB absolute error e_k as defined in (11). This has the disadvantage of not being normalized and therefore it depends on the transmitted power; in consequence, for higher P_n the SINRs and the magnitude of the corresponding SINR absolute errors are higher too. Nevertheless, this metric, contrary to, for example, the relative error, can be translated directly into the margin necessary to subtract from the SINR estimated by the gateway, $\hat{\text{SINR}}_k$, in order to guarantee a robust transmission. To obtain meaningful results with the SINR absolute error, the operation point is selected carefully to reflect a close to reality system.

III. Nullification description

Precoding requires the transmitter to have knowledge of the users channel in the form of CSIT (Channel State Information at the Transmitter), since this is necessary to compute the precoding matrix $\mathbf{W}$ and estimate the precoded SINR of each user. The CSIT available at the gateway is usually imperfect, among other things, due to errors in the estimation of the coefficients of the CSI vectors per the users. However, the main cause of degradation of the CSI is the nullification effect. This is the inability of a receiver to estimate some of the coefficients of the CSI vector due to the low received power of the interfering beams. Thus, a large number of coefficients of the CSI matrix which is used by the gateway are unknown and replaced by zeros. This channel matrix, $\hat{\mathbf{H}}$, is said to have nullification errors.

Regarding the synchronization of the carriers transmitted by the beams, two types of satellite systems can be considered, with different consequences on the CSI estimation and nullification. With network synchronization [12], the waveforms received by the user, the desired carrier and the interfering carriers from adjacent beams, can be considered synchronous, i.e. the time delays between the different waveforms is much lower than the symbol period. In the specific case of DVB-S2X, with orthogonal Walsh-Hadamard (WH) sequences for the P pilots, the detection of the interfering carriers is limited mainly by the noise. The P pilots are sequences of known non-precoded symbols which receivers use to estimate the CSI, since the orthogonal WH sequences enable to differentiate up to 31 different interfering carriers. In this situation, the periodical repetition of the 36-pilots blocks along the bundled PLFRAME allows the detection of interfering carriers whose power is even 15 dB below the noise. If pilots across more than one superframe are averaged, this threshold can be further reduced. When the carriers are not synchronized, the orthogonality of the WH sequences can not be exploited, and the estimation becomes limited fundamentally by the interference [13]. In this asynchronous system, interfering carriers can be estimated even when they are approximately up to 15 dB below the desired carrier. Recent research showed that for levering all the potential of precoding in multibeam satellite systems the carriers should be synchronized to a great extent [12].

Mathematically, for simulating the nullification effect under purely asynchronous or synchronous carriers, we construct the nullified matrix $\hat{\mathbf{H}}$ in two different forms, depending on the system type:

1) **Asynchronous system**: Since our assumption is to work in clear sky conditions, the precoded C/N is relatively high so that the nullification in the asynchronous sytem is driven mainly by the interference power more than the noise power. Therefore we assume that the nullification is performed based on a I/C threshold T_h:

$$\hat{h}_{ij} = \begin{cases} 0 & \text{if} \quad 20\log_{10}|h_{ij}/h_{ii}| < T_h \\ h_{ij}, & \text{otherwise.} \end{cases} \tag{12}$$

2) **Synchronous system**: the nullification is performed based on a I/N threshold T_h:

$$\hat{h}_{ij} = \begin{cases} 0 & \text{if} \quad 20\log_{10}\sqrt{\mathsf{snr}}|h_{ij}| < T_h \\ h_{ij}, & \text{otherwise.} \end{cases} \tag{13}$$

In practice, the satellite networks are not fully asynchronous or synchronous, and the capability of a practical receiver to estimate a given interfering carrier depends on both C/N and C/I. Fig. 2 shows the (C/N, C/I) regions for which estimation is possible and for which nullification takes place. This performance of the CSI estimation is achieved by using the architecture shown in Fig. 1 and is referred hereafter as real nullification. The number of estimated carriers per position with the real nullification depicted in Fig. 2, and for the system parameters of Tab. II, ranges between 1 and 15. In the edge of the satellite coverage typically less than 6 carriers are estimated and far from the edges this number increases, lying between 10 and 15. This last number is the half of the maximum number of carriers which can be differentiated with the WH sequences (32) and much lower than the number of total beams, 245. Furthermore, the results obtained in the simulations with real nullification contain also Gaussian random CSI estimation errors. These errors are larger when the operating C/N and C/I are closer to the non-detection region. Their maximum and typical values are tabulated in Tab. I.

The value of channel h_{ij}, which is obtained from the beam pattern, is modified not only for accounting the nullification but also to take into account estimation errors in the amplitude and phase of the channel coefficients. For the amplitude, the mean error and the standard deviation are shown in Tab. I in relative terms, to be independent of the magnitude of the channel coefficients. On the other hand, the mean and standard deviation of the phase estimation errors are shown in absolute terms in Tab. I.

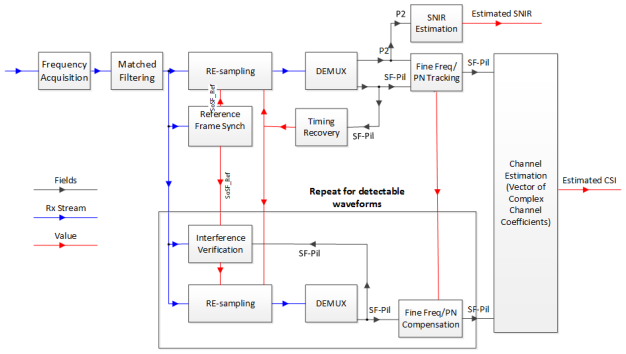

Fig. 1: Architecture of the receiver for CSI detection and estimation.

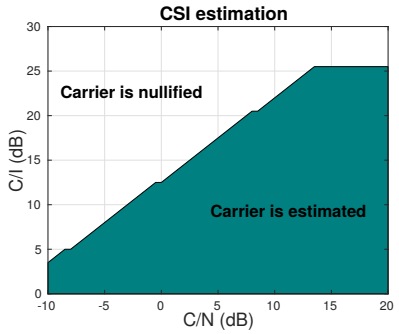

Fig. 2: Range of values of C/N and C/I which allow carriers estimation in real nullification.

Amplitude $|h_{ij}|$

Mean relative error	Maximum: 0.17	Typical: 0.05
Relative standard deviation	Maximum: 0.02	Typical: 0.005

Phase $\angle\, h_{ij}(^o)$

Mean error	Maximum: 3^o	Typical: 0^o
Standard deviation	Maximum: 1.2^o	Typical: 0.7^o

TABLE I: Characterization of the CSI estimation errors.

IV. Nullification error evaluation

In this section simulation results of the SINR absolute error due to nullification and CSI estimation errors will be provided from three different perspectives. Firstly, subection IV-A presents several statistics of the aggregated SINR error, analysing it in global way mixing different positions of all the beams of the satellite. Then, subsection IV-B analyses the SINR absolute error adding the spatial dimension of the data in order to reveal the geographical dependence of the error. Lastly, subsection IV-C focus the attention on the statistics of the SINR and the SINR absolute error from the point of view of specific users.

The main parameters of the Ka-band multibeam satellite system used in the simulations are collected in Table II. With these parameters the clear sky non-precoded C/N of the users ranges from 7 to 13.75 dB, and from 11 to 13.75 dB in the case of users located at the beam center.

Parameter	**Value**
Satellite orbit	GEO
Downlink frequency	Ka-band (20 GHz)
Number of beams	245
Receive antenna gain	40 dBi
T Noise temperature	235.3 K
Receiver G/T	16.3 dB/K
B Noise bandwidth (roll-off included)	12 MHz
P_n Per beam and polarization transmit power	0.15 W (21.76 dBm)
Total power	36.75 W (15.65 dBW)

TABLE II: System parameters.

A. Aggregated results

In this subsection a collection of results of the SINR absolute error, as defined in Equation (11), is presented. All of them are obtained with a MMSE precoder using SPC normalization under random scheduling with four different sets of scheduled users. These can be selected from the positions within a circle centred at each beam center and with a radius lower than $2/6$, $3/6$ or $4/6$ of the beam radius, or well among all the beam positions. The selection of the users has an impact on the magnitude of the errors, as it will be shown later, and it can give us some idea of the lower and upper bound of the SINR absolute error in a real precoded system where scheduling is an indispensable component. Each simulation comprises 500 realizations. In each one a random user is selected within each beam, then the channel matrix $\mathbf{H}$ is built using the channel instances of the scheduled users and its nullified version $\hat{\mathbf{H}}$ is obtained. After that, the precoding matrix $\mathbf{W}$ is calculated prior to the computation of the actual UT SINRs SINR_k and estimated by the gateway $\widehat{\text{SINR}}_k$. Lastly, its difference gives the SINR absolute error e_k, which is analysed globally in this subsection, after mixing the data from all the beams.

Firstly, the bar diagrams of Fig. 3a show the maximum SINR absolute error by using the simple model for synchronous nullification of Equation (2) as a function of the set of scheduled users. Four different I/N nullification thresholds are studied in order to link the performance in the interfering carriers detection with the maximum SINR error obtained. In the light of data from Fig. 3a, for the maximum SINR error being lower than 1 dB an I/N between -15 and -20 dB is needed in synchronous systems. CSI detection can be improved, with the ensuing reduction of the SINR error, by averaging the pilot symbols during longer periods.

Now, Fig. 3b is focused on the results obtained with a realistic nullification which takes into account both C/N and C/I, as depicted in Fig. 2. Fig. 3b contains the bar diagrams of the maximum error with the real nullification in the middle. Results for an asynchronous nullification with I/C threshold

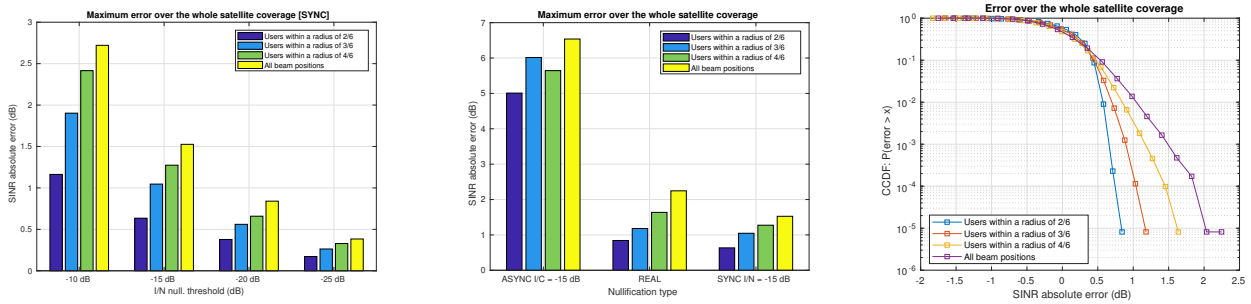

(a) Synchronous nullification

(b) Asynchronous, real and synchronous nullification

(c) SINR error CCDF with real nullification

Fig. 3: Maximum SINR absolute error over 500 realizations in (a) and (b), and CCDF of the SINR absolute error with real nullification in (c). All results were obtained with MMSE precoder and SPC normalization.

of -15 dB and synchronous with I/N threshold of -15 dB are also shown for comparison. As it can be observed, the errors with the real nullification are halfway between the other two. The SINR maximum errors with the real nullification fall between 0.84 and 2.25 dB depending on the set of users scheduled. As can be seen, the error increases when the area of scheduled users becomes wider. The reason is that the power imbalance among the scheduled users amplifies the errors introduced by the nullification of the CSI. As the area gets larger, the variance of the C/N of the different scheduled users increases accordingly. Moreover, when the order of the system is reduced, considering for example only a cluster of 9 beams, the error becomes lower. Reductions of 0.5 dB can be observed, depending on the particular beams selected and the group of scheduled users.

Fig. 3c shows the experimental Complementary Cumulative Distribution Function (CCDF) of the SINR error in the simulations with the real nullification. The CCDF provides the probability of the SINR error being larger than a given abscissa value and offers some insight into the value of the margin required for guaranteeing a given target Frame Error Rate (FER) throughout all the satellite footprint.

These results show that even in the absence of other imperfections, nullification itself can degrade the performance of multibeam satellite systems which use precoding unless proper countermeasures are applied. An error larger than 0 dB means that the gateway is overestimating the actual UT SINR, and it implies that if $\widehat{\text{SINR}}_k$ is used directly to allocate a MCS to the UT at beam k, an error in the transmission will occur whenever the error is bigger than the distance of $\widehat{\text{SINR}}_k$ to the threshold SINR of the MCS used in the transmitted frame. And since the spacing between two DVB-S2X consecutive MCS is typically between 0.3 and 1.0 dB and as the SINR errors exceed this values with a non-negligible probability, the FER will be higher than the QEF target of 10^{-5}, one erroneous frame out of $100,000$.

B. Spatial analysis

In order to establish the existence of a potential geographical dependence of the SINR absolute error e_k, the following two experiments were performed. The simulations comprise $1,000$ realizations, i.e., transmitted frames, and in each realization a user is selected randomly among the positions within a circle centred at each beam center and with a normalized radius lower than $2/6$ or $4/6$, depending on the simulation. For each realization the error in all the 245 beams is calculated, and the maximum error within each beam is obtained and represented in a map. Only the map with the first case is included since the conclusions drawn from both are the same.

The map in Fig. 4 shows how the maximum SINR error is not the same in all the beams but, rather, has a spatial distribution. Error tends to be larger in those beams located at the center of the satellite coverage whilst in the edge of the coverage the error is usually lower. The difference between the maximum error in the center and the periphery reach values as high as 1.4 dB. These differences among the errors in different beams have also been found even when PLPC normalization is used to set the same transmit power for all the beams.

Moreover, within a given beam there are also remarkable differences in the maximum SINR error among the different positions. Although there is not a clear and constant pattern of the error distribution inside a beam, differences in the maximum SINR error among positions of the same beam are also in the order of 1.4-1.6 dB.

A rough countermeasure for the errors caused by the nullification comes from the subtraction of a global margin to the SINRs estimated by the gateway. This margin could be obtained from the CCDF of the SINR absolute error (shown in Fig. 3c), by using the target FER. However, the results of the geographical distribution of the error show that a global margin to be applied throughout the whole footprint can be quite inefficient, since the error magnitude differs significantly across the footprint. Furthermore, remarkable differences appear within the same beam from one position to another. As a result, a per user margin seems a better solution.

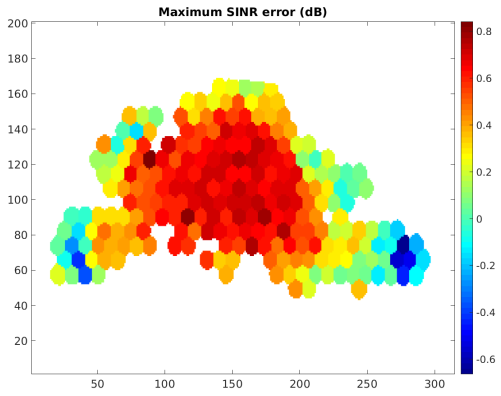

Fig. 4: Map of the SINR maximum error per beam over 1,000 realizations with MMSE-SPC precoder, real nullification and scheduling users from the central positions of the beams (radius lower than 2/6).

C. Statistical analysis at fixed locations

This subsection deals with the characterization of the SINR and the associated error in specific positions as function of the location of the users scheduled in other beams. If a user is always scheduled together with the same set of users in all the other 244 beams, the SINR and the SINR absolute error will be constant with time in the absence of other imperfections such as channel fading, phase noise or Gaussian estimation errors in the CSI. However, the user grouping is not kept fixed with time. Although the scheduler builds groups of users which are more likely to be scheduled together, no fixed grouping is possible due to the random nature of the users traffic.

Here, for each simulated UT on a given location, two types of beams are differentiated, namely, the 6 beams in the first tier surrounding the user beam, the neighbour beams of the UT, and the rest of the beams. In order to account for the fact that a UT tends to be scheduled with the same group of users in its surrounding beams, we always schedule the UT located at the center of the 6 surrounding beams, whereas four different location policies are applied for the rest of the beams: selection of the central user of the beam, or selection of users randomly within the circle of radius $2/6$, $3/6$ or $4/6$ as explained in Section IV-A. With this, the SINR of the UT under analysis together with its absolute error are calculated for $2,000$ realizations.

Fig. 5 shows the histograms with the distribution of the SINR absolute error and the SINR for one UT, located in beam 213, depending on the scheduling policy for the non-neighbour beams. The same scale in the abscissa is axis is employed in all the cases to ease the comparison. It was found that the SINR absolute error follows a Gaussian distribution for practically all the cases studied (several UTs located in different part of the beam and in different beams of the coverage). Fig. 5a collects the four histograms of the error with its Gaussian fit in red for this particular UT depending of the scheduling policies of the remaining non-neighbour beams. The first observation is that the SINR absolute error follows quite closely a Gaussian distribution in the four cases. The second observation is that the variance of the error grows as the users scheduled in the remaining beams can belong to a larger circle. Lastly, although in this particular example this is not totally satisfied, in the vast majority of the UTs analysed the average of the error remains fixed, independent of the policy applied for selecting the users in the remaining beams.

On the other side, Fig. 5b shows the distribution of the actual SINR of the same fixed user with respect to the selection policy of the users in the non-neighbour beams. Again, it can be said that the distribution of the SINRs is nearly Gaussian. Looking at the variance, we observe that it also increases when the users scheduled in the remote beams can be located farther away from their respective beam centers. As last remark, and in addition to the variance increase, if the users of the non-neighbour beams are selected within a larger circle, the values or the SINR are also reduced with respect to those when all the other users of the system are located at the beam center (marked with a blue circle). Regarding the variability observed in the upperleft histogram (when all the other users, except the UT under analysis, are located at the beam center) this is due to the CSI random estimation errors and the phase noise of the payload (different in each realization) which are assumed throughout this work.

V. Link Adaptation

In this section we introduce a simple link adaptation algorithm for a full-frequency reuse satellite system based on the use of an adaptive margin as a countermeasure for the errors that nullification and CSI estimation can cause. The algorithm performance will be evaluated through simulations. The aim of the algorithm is to select the MCS for each UT maintaining the FER around a very low target value p_0. The link adaptation procedure must be performed at the gateway side rather than the UTs, since the gateway is the only entity with all the required information, namely, channel vector of all scheduled users and precoding matrix employed in each frame. Since the SINR absolute error due to nullification changes from one position to another, and results change significantly for different UTs location, the gateway will run one independent margin per UT.

A. Algorithm description

We assume that for each received frame the UTs feedback the outcome of the frame decoding to the gateway, which will be used later to update the margin of each user. This variable ϵ_i takes the value 1 to indicate that an error has occurred and the frame i could not be decoded (NAK), and it takes the value 0 to indicate that frame i was decoded successfully (ACK). We should note that the ACK/NAK feedback is used only for adapting the margins of the link adaptation algorithms, and there is not any retransmission of the frames at the physical layer due to the long propagation delay.

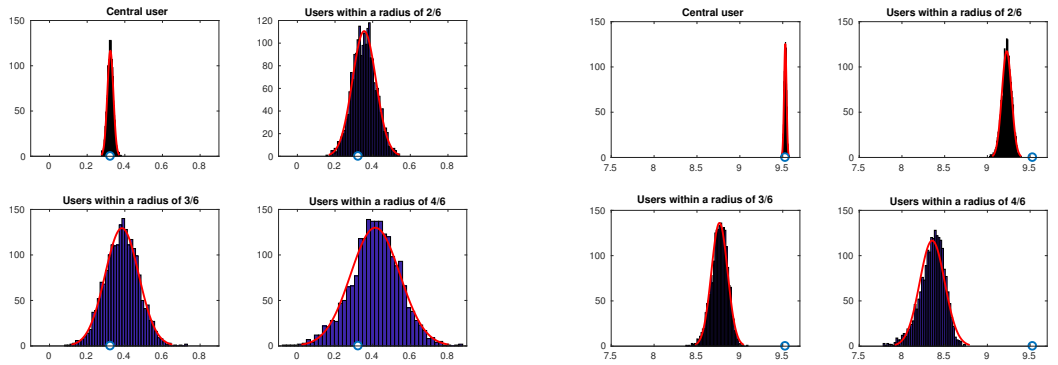

(a) SINR absolute error histogram and Gausian fit.

(b) Actual UT SINR histogram and Gaussian fit.

Fig. 5: SINR absolute error and actual SINR UT histograms with their Gaussian fit. Scheduling policy: central user in the tier of 6 neighbour beams, and four different selection criteria in the rest of beams.

The selection of the MCS of user k at time instant i, $\text{MCS}_{k,i}$, is done with a Lookup Table (LUT) whose input is the estimation of the SINR of user k, $\widehat{\text{SINR}}_k$, performed by the gateway with the imperfect CSIT, plus an adaptive margin $m_{k,i}$ as done in [8]:

$$\text{MCS}_{k,i} = \Pi\left(\widehat{\text{SINR}}_{k,i} + m_{k,i}\right). \tag{14}$$

The function $\Pi(\cdot)$ is a staircase function which maps SINR intervals to MCS following the performance tables of the DVB-S2X standard [1]. The reverse operation is done by means of the function $\amalg(\cdot)$, which returns the threshold SINR of a given MCS.

In the simulations we consider that a decoding error event occurs whenever the actual SINR at the UT is lower than the SINR threshold of the MODCOD used to transmit that frame. Using the indicator function $[\cdot]$, this is expressed as

$$\epsilon_{k,i} = [\underbrace{\text{SINR}_{k,i}}_{\text{Actual SINR}} < \underbrace{\amalg\left(\text{MCS}_{k,i}\right)}_{\text{Threshold SINR of MCS used}}]. \tag{15}$$

The gateway receives the feedback form each user and updates each user margin independently using the following recursive equation

$$m_{k,i+1} = m_{k,i} - \mu\left(\epsilon_{k,i} - p_0\right), \tag{16}$$

where μ is the adaptation step, smaller than one, and p_0 the target FER. In this way, depending on the decodification outcome two situations are possible:

- If no error occurs (ACK), then the margin is incremented by a 'small' quantity $\Delta_{ACK} = \mu p_0$.
- If an error ocurrs (NAK), then the margin is decremented by a larger amount: $\Delta_{NAK} = \mu(1-p_0)$, which for small values of the target FER becomes approximately μ.

The ratio between the margin increment and decrement following an ACK and a NAK, respectively, depends on the target FER and it is equal to $\Delta_{ACK}/\Delta_{NAK} = p_0/(1-p_0)$. This guarantees that when the margin converges to the optimum value which ensures the target FER, it remains oscillating around that value. The lower the FER p_0, the margin needs more time to converge to its final value, therefore, in order to speed up the convergence time, a smart initialization of the margin of each user could be applied by using a priori information of the geographical distribution of the SINR error. Furthermore, some variants of this classic algorithm of the adaptive margin for Outer Loop Link Adaptation (OLLA), like that introduced in [14] for speed up the convergence without losing performance in steady state, could be applied, although they are not evaluated here.

B. Simulation results

10 different beams, far apart from each other, are chosen with a user randomly located at each beam. The rest of the beams are divided into two groups, the 6 neighbour beams which are in contact with the 10 selected beams and all the rest of beams. In all the neighbour beams the central user is always scheduled, to emulate the fact that the UTs under analysis tend to be scheduled with the same group of users in the beams around them. And in all the non-neighbour beams random locations are chosen from the circles of normalized radius $2/6$ or $4/6$, depending on the particular simulation. In each realization the users of the non-neighbour beams are randomly selected, the channel matrix $\mathbf{H}$ and its version after real nullification, $\hat{\mathbf{H}}$, are computed, and the MMSE-SPC precoding matrix is computed. The link adaptation algorithm introduced earlier is then used to select the MCS to employ in the transmission to the 10 UTs under analysis by using an independent margin for each user. Equation (15) is used to decide the outcome of each frame decoding (success or not) by using the actual UTs SINRs (calculated with equation (7)). With the decoding outcomes the margins of the 10 UTs are updated using (16), margins to be applied in the next realization. At the end of the simulation the FER of the UTs after the margin converges is calculated.

The value taken by the adaptation step μ in (16) is 0.01 and three different target FERs p_0 were evaluated, namely 10^{-3}, 10^{-4} and 10^{-5}, this last value corresponding to the QEF FER target of DVB-S2X. The number of realizations (transmitted frames) were $100,000$, $500,000$ and $2,000,000$ respectively for each target FER. In addition, all the 10 margins were initialized to zero. In all the simulations it was found that the experimental FER matched the target, being within the range 90% to 110% of the target value p_0. However, not applying any margin to the SINRs calculated by the gateway results in inadmissible FER, much larger than 10^{-5}, being this even higher than 10% in half of our simulations. The only impairment considered in these simulations was the nullification effect in the CSI estimation by the receivers, with the performance shown in Fig. 2, referred throughout this work as real nullification. The link adaptation algorithm based on an adaptive margin per user, updated with the feedback of the ACK/NAK of the frames intended to each UT, shows to be a useful countermeasure for the errors introduced by the nullification since it maintains the FER of the UTs at the required target value, with the minimum performance loss. In a real system the function of the link adaptation algorithm, in addition to account for the errors due to the nullification of the CSI, as it is analysed in this paper, is to address varying channel conditions, channel estimation errors and outdated CSIT.

VI. Conclusion

The problem of the CSI detection error was introduced, showing that it causes errors in the precoded SINR of the users which the gateway must calculate to perform MCS allocation. This leads to the increment of the rate of erroneous frames if no proper countermeasure is applied. The study of the SINR absolute error revealed that there are important differences in the maximum error among different beams, and even among different positions within the same beam. It was shown also that, under certain conditions, this error can be modeled as a Gaussian random variable. In order to ensure the robustness of the communications the use of an adaptive margin was proposed. This helps to counteract the errors in the SINR of the users which is estimated by the gateway. This margin, independent for each UT, is updated by the gateway based on the ACK/NAK feedback from the users and is employed in the link adaptation for MCS selection. Simulation results showed that by using this link adaptation algorithm, the QEF condition can be achieved, even in the presence of SINR calculation errors due to the non-detection of some components of the CSI.

Acknowledgement

This work was funded by the Xunta de Galicia (Secretaria Xeral de Universidades) under a predoctoral scholarship (co-funded by the European Social Fund) and under Agrupación Estratéxica Consolidada de Galicia accreditation 2016-2019 (co-funded by the European Regional Development Fund - ERDF). The research was done during a stay at the Interdisciplinary Centre for Security, Reliability and Trust (SnT), University of Luxembourg, supported by the project SatNEx-IV, co-funded by the European Space Agency (ESA). The view expressed herein can in no way be taken to reflect the official opinion of the European Space Agency.

References

[1] "Digital Video Broadcasting (DVB); Second generation framing structure, channel coding and modulation systems for Broadcasting, Interactive Services, News Gathering and other broadband satellite applications; Part 2: DVB-S2 Extensions (DVB-S2X)," *ETSI EN 302 307-2 V1.1.1 (2014-10)*.

[2] O. Vidal, J. Lacan, J. Radzik, E. Alberty, and P. Inigo, "Linear Precoding performance analysis in a Broadband satellite system with a 2-color dual-polarization reuse scheme," *31st AIAA International Communications Satellite Systems Conference, International Communications Satellite Systems Conferences (ICSSC), American Institute of Aeronautics and Astronautics*, 2013.

[3] D. Christopoulos, S. Chatzinotas, and B. Ottersten, "Multicast multigroup precoding and user scheduling for frame-based satellite communications," *IEEE Transactions on Wireless Communications*, vol. 14, no. 9, pp. 4695–4707, Sept 2015.

[4] G. Taricco, "Linear precoding methods for multi-beam broadband satellite systems," in *European Wireless 2014; 20th European Wireless Conference*, May 2014, pp. 1–6.

[5] M. A. Vazquez, A. Perez-Neira, D. Christopoulos, S. Chatzinotas, B. Ottersten, P. D. Arapoglou, A. Ginesi, and G. Taricco, "Precoding in multibeam satellite communications: Present and future challenges," *IEEE Wireless Communications*, vol. 23, no. 6, pp. 88–95, December 2016.

[6] M. Vazquez, B. Shankar, C. Kourogiorgas, P. Arapoglou, V. Icolari, S. Chatzinotas, A. Panagopoulos, and A. Perez-Neira, "Precoding, Scheduling and Link Adaptation in Mobile Interactive Multibeam Satellite Systems," *IEEE Journal on Selected Areas in Communications*, 2018.

[7] S. Andrenacci, D. Spano, D. Christopoulos, S. Chatzinotas, J. Krause, and B. Ottersten, "Optimized link adaptation for DVB-S2X precoded waveforms based on SNIR estimation," in *2016 50th Asilomar Conference on Signals, Systems and Computers*, Nov 2016, pp. 502–506.

[8] A. Rico-Alvarino, A. Tato, and C. Mosquera, "Robust adaptive coding and modulation scheme for the mobile satellite forward link," in *Signal Processing Advances in Wireless Communications (SPAWC), 2015 IEEE 15th International Workshop on*, June 2015.

[9] A. Tato, P. Henarejos, C. Mosquera, and A. Pérez-Neira, "Link Adaptation Algorithms for Dual Polarization Mobile Satellite Systems," in *Wireless and Satellite Systems*, P. Pillai, K. Sithamparanathan, G. Giambene, M. Á. Vázquez, and P. D. Mitchell, Eds. Cham: Springer International Publishing, 2018, pp. 52–61.

[10] D. Christopoulos, P.-D. Arapoglou, and S. Chatzinotas, "Linear Precoding in Multibeam SatComs: Practical Constraints," in *31st AIAA International Communications Satellite Systems Conference, International Communications Satellite Systems Conferences (ICSSC)*, A. I. of Aeronautics and Astronautics, Eds., 2013.

[11] Y. Jiang, M. K. Varanasi, and J. Li, "Performance Analysis of ZF and MMSE Equalizers for MIMO Systems: An In-Depth Study of the High SNR Regime," *IEEE Transactions on Information Theory*, vol. 57, no. 4, pp. 2008–2026, April 2011.

[12] S. Andrenacci, S. Chatzinotas, A. Vanelli-Coralli, S. Cioni, A. Ginesi, and B. Ottersten, "Exploiting orthogonality in DVB-S2X through timing pre-compensation," in *2016 8th Advanced Satellite Multimedia Systems Conference and the 14th Signal Processing for Space Communications Workshop (ASMS/SPSC)*, Sept 2016, pp. 1–8.

[13] P.-D. Arapoglou, A. Ginesi, S. Cioni, S. Erl, F. Clazzer, S. Andrenacci, and A. Vanelli-Coralli, "DVB-S2X-enabled Precoding for High Throughput Satellite Systems," *Int. J. Satell. Commun. Netw.*, vol. 34, no. 3, pp. 439–455, May 2016. [Online]. Available: https://doi.org/10.1002/sat.1122

[14] R. A. Delgado, K. Lau, R. Middleton, R. S. Karlsson, T. Wigren, and Y. Sun, "Fast convergence outer loop link adaptation with infrequent updates in steady state," in *2017 IEEE 86th Vehicular Technology Conference (VTC-Fall)*, Sept 2017, pp. 1–5.